Numerical Simulations for ITER Divertor Armour Erosion and SOL Contamination due to Disruptions and ELMs

I.S. Landman, S.E. Pestchanyi, B.N. Bazylev

Forschungszentrum Karlsruhe, Institute for Pulsed Power and Microwave Technology,
P. B. 3640, 76021 Karlsruhe, Germany

E-mail contact of main author: igor.landman@ihm.fzk.de

Abstract. The divertor armour materials for ITER are going to be tungsten (as brushe or plates) and CFC. Disruptive loads with the heat deposition Q up to 30 MJ/m^2 on the time scale τ of 3 ms or operation with ELMs at repetitive loads of $Q \sim 3$ MJ/m^2 and $\tau \sim 0.3$ ms cause enhanced armour erosion and produce contamination of SOL. Recent numerical investigations of erosion mechanisms with the anisotropic thermomechanics code PEGASUS−3D and the surface melt motion code MEMOS−1.5D as well as hot hydrogen plasma dynamics, heat loads at the armour surface and backward propagation of material plasma in SOL with the radiation-magnetohydrodynamics code FOREV−2D are survived. For CFC targets, the local overheating model is explained and numerically demonstrated. For the tungsten targets the numerical analysis of melt motion erosion of W-brushe and bulk tungsten targets on the base of MEMOS−1.5D calculations is developed and accompanied by numerical results. For validation of the codes at the regimes relevant to ITER disruptions and ELMs, the simulation results are compared with available experiments carried out at plasma guns, electron beam test facilities and the tokamak JET.

1. Introduction

The ELMy H-mode of ITER operation is preferable for demonstration of technological advantages of thermonuclear power production on a full scale. However, the high power transient processes in ITER such as bursts of edge localized modes (ELMs) that accompany with the frequency of 1-10^2 Hz the normal tokamak operation and the disruptions that sometimes interrupt the quasi-stationary discharge will be probably much more serious problem than in the available tokamaks. The heat deposition Q in the range about 0.5 – 3 MJ/m^2 on the time scale τ about 0.1 – 0.5 ms for ELMs and $Q \sim 10 – 30$ MJ/m^2 at $\tau \sim 1 – 10$ ms for the disruptions are expected at the divertor surface [1]. Each ELM with such parameters provides a heat load that causes intense vaporization at the armour surface. Influence of the divertor armour material plasma upon the confined DT-plasma is a key issue for fusion technology, because contamination of the core plasma may result in the radiation collapse of the confinement, and intense radiation impact on the first wall – in its damage. The plasma facing components (PFC) of the ITER divertor are going to be made of carbon fibre composites (CFC) in the most loaded part at the separatrix strike position (SSP) and of tungsten (W-brushe) in the other parts. The large loads can cause surface erosion of the armour and evaporation of a thin layer of the material that after ionization in the impacting plasma stream acts as a plasma shield which simultaneously propagates in the scrape-off layer (SOL).

This work surveys latter theoretical investigations carried out in FZK for the divertor armour damages and the impurity propagation in SOL applying and upgrading earlier developed codes. The only way to obtain confidence of the used assumptions and theoretical models is a validation of the modelling by experiments, because in reality unexpected physical processes might play an important role. Therefore non-tokamak validation experiments have been engaged. The validation of the code against experiments on the plasma guns [2-4] has been carried out.

The computational tool applied for direct calculation of wall loads and plasma processes is two-dimensional (2D) RMHD (radiation-magneto-hydrodynamics) code FOREV–2D [5]. ITER relevant simulations with it for SOL are described in Section 2. For simulation of the damage to tungsten surfaces the incompressible fluid dynamics code MEMOS-1.5D [6] is applied. The simulations with MEMOS-1.5D are presented in Section 3. For PFC made of carbon-based materials the main erosion effect under the high heat fluxes is brittle destruction. In this case the thermomechanics code PEGASUS-3D [7] was applied. The brittle destruction simulations are described in Section 4.

2. Simulation of SOL plasma with FOREV-2D

The code FOREV-2D models the hot plasma lost across the separatrix into SOL during a transient event, its propagation towards the wall and impact on the armour, accounting for a self-consistent evaporation, ionization of carbon-, tungsten- and beryllium atoms, the radiation transport in the contaminated plasma and backward propagation of the erosion products into SOL. Earlier the code was created having slab geometry and one-fluid plasma implemented, which was sufficient for simulation of consequences of disruptions when a dense plasma shield of the density above 10^{21} m^{-3} forms in front of the surface [5]. Recently FOREV-2D was upgraded for adequate tokamak relevant simulations at lower heat fluxes corresponding to ELMs [8,9]. Toroidal magnetic field geometry with single poloidal field null and one divertor, the whole SOL, inner- and outer divertor plates are implemented. The ion fluids of D, T, He, He^+ and all charge states of the light impurities such as C or Be can be simultaneously simulated. For estimation of carbon plasma transport and cooling properties of the plasma in SOL and pedestal region radiation transport algorithm in FOREV-2D code has also been upgraded. The modification concerns further development of the former forward-reverse technique from rectangular coordinates and rectangular meshes to curvilinear coordinates and arbitrary skewed tetragonal meshes. Here the radiation feature is highlighted.

Radiation transport due to impurities is a complex nonlinear problem. For reliable simulation of the radiation cooling, numerical results have to be verified by some experiments on the existing tokamaks. From these only JET seems powerful enough for producing giant ELMs that can evaporate CFC armour and pollute the hydrogen plasma of pedestal. Therefore JET relevant calculations for a giant ELM of ~1 MJ size have been performed. In the ELM scenario the hot plasma losses from the pedestal region through the separatrix with a rate

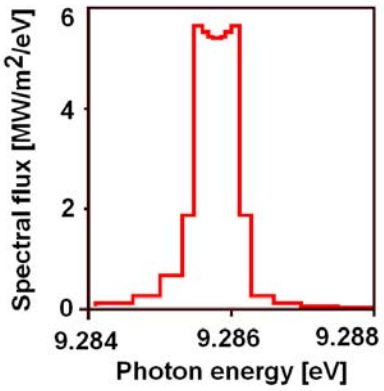

FIG. 1. Spectral radiation flux in vicinity of one strong line: reabsorption effect is seen as a decrease of intensity in the line centre

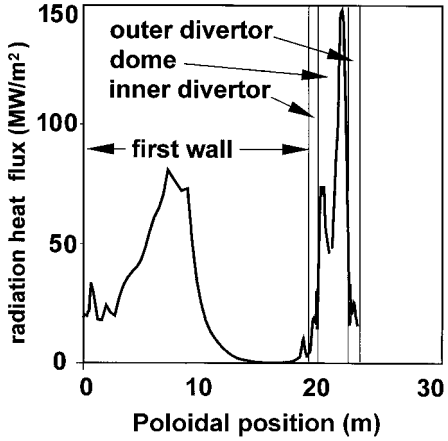

FIG. 2 Radiation load onto ITER vessel walls (results of FOREV-2D)

determined by a specified Q and τ. It is assumed that the lost plasma appears then in SOL having an exponential density profile with some maximum density at the separatrix. The hot plasma propagates towards the CFC divertor armour legs, heats them and causes vaporization at their surfaces. The carbon vapour propagates backwards finally filling the whole SOL. The numerical results are compared with the available experimental data. Unfortunately, the available experimental data have very rough time resolution for ELM description. Nevertheless, based on this comparison first code validation is done. According to the simulation, the main contribution to the radiation flux arises from a few strong carbon lines. For adequate simulation of line radiation the opacity data of FOREV have been upgraded to better resolve their line shapes. The radiation at the main lines centre is obtained to be substantially reabsorbed which deforms the line profiles (see Fig.1). Simulation of ELM in JET using the proposed ELM scenario and improved opacity tables resulted in a reasonable agreement with measured total cooling rate of 20 MW, but the calculated cooling rate of 35-50 MW obtained in the simulation is strongly dependent on the ELM scenario.

Several simulations of type I ELMs in ITER at Q = 1-3 MJ/m^2 and τ = 0.1-0.5 ms carried out in [9] revealed that there are two different regimes of radiative cooling. First of them can be characterised by low carbon plasma temperature less than 6 eV and high cooling rate, when all the heating power from the pedestal plasma is dissipated by radiation and the impurity temperature keeps low. In this regime the radiative cooling rate can be comparable with the ITER fusion power of 0.5 GW. The second regime occurs when the carbon density is low. The heating power becomes to be sufficient to overcome the radiation barrier. In this case the carbon plasma temperature increases up to 40-50 eV and the radiative cooling becomes 2-3 orders of magnitude lower than that in the first regime. The carbon impurity absorbs about 1 keV per carbon atom, spending the energy for ionisation.

Typical radiation flux distribution calculated at the first wall is shown in Fig. 2 corresponding to a time moment when the carbon plasma is distributed almost uniformly along the separatrix in SOL and in the divertor legs. The maximal radiation heat load is on the dome and adjoining parts of divertor most filled with the radiative impurity. A smaller peak of the radiation flux is seen at the top of the main chamber, where the plasma thickness is rather large due to a divergence of the poloidal magnetic field.

3. Melting of W-brush's surfaces

The main disadvantage of bulk tungsten armour is surface cracking under the high heat loads typical for the intense transient events with $Q > 1$ MJ/m^2 and $\tau > 0.1$ ms. One possibility to mitigate the surface cracking is the tungsten macrobrush armour (W-brushe). For the disruptions the most important mechanisms of metallic armour damage are surface melting and melt splashing [6]. Single giant ELMs also result in melting and evaporation, and in the vapour shield which generates the motion of the melt layer due to pressure gradient along the target surface. However, because of a rather short time of ELMs and moderate velocities of melt motion the melt splashing seems to be negligible [10].

The melt layer erosion of the bulk tungsten armour under the heat loads caused by single and multiple transient events was numerically investigated using the code MEMOS-1.5D [6,10-12]. In assumption of the flat melt surfaces the melt motion in MEMOS-1.5D is described in the "shallow water" approximation, with the surface tension, viscosity of molten metal, and the radiative losses from the hot surface taken into account. The plasma pressure gradient along the divertor plate, the gradient of surface tension and the Lorentz force cause the melt

acceleration. A two-dimensional heat transport equation with two boundary conditions at the moving vapour-liquid- and liquid-solid interfaces describes the temperature inside the target. Temperature dependent thermophysical data are used. Now the main results are summarized.

The numerical simulation of melt erosion of bulk tungsten armour demonstrated that the depth of melt pool is always below 400 μm for disruptions and below 80 μm for giant ELMs. The pressure gradient of the plasma shield is mainly responsible for an intensive melt motion with the melt velocities up to several tens cm/s; the Lorentz force slightly intensifies the melt motion. The surface roughness is of a fraction of μm for moderate ELMs, it reaches 1 μm in the case of giant ELMs and increases up to ~70 μm for long time disruptions. For all transient events the depth of melt pool and the depth of final erosion crater is much less than typical sizes of macrobrush elements with the brush diameter of 1cm, the gap width of 0.3 – 1 mm and the gap depth of 1 cm. Thus the "shallow water" approximation for W-brush targets is valid. To take into account the main features of the macrobrush geometry the code MEMOS has been upgraded [13]. For avoiding sharp brush edges it is assumed that their shape is an arc of a radius R of about 1 mm. For the macrobrush target a continuous surface consisting of a sequence of the top-brush sections, the circular segments, the lateral-brush sections, and the gap-bottom sections is implemented. A non-uniform curvilinear orthogonal numerical grid (x,z) with the coordinate x along the surface and the coordinate z directed inside the target fits the whole surface. It is assumed that the melt moves always along the surface without separation from the melt bottom and without droplet formation, including the arc segments between the tops of W-brushes and their lateral surfaces. The value of the melt velocity is assumed constant at the edge arcs where the centrifugal force appears. The tangential friction force appearing due to the momentum transfer from inclined plasma stream dumped onto the target surface is included. Distributions of the heat load and the plasma pressure at all macrobrush elements are recalculated taking into account the geometric features of the target and plasma shield. The heat loads at the lateral surfaces are determined by the radiation from the shielding layer.

The first validation of the code is performed against experiments on W-macrobrush target erosion under repetitive plasma loads of for the heat load at QSPA plasma gun facility [12,13]. A castellated tungsten target consisting of separate elements of sizes D of 10x10x3 mm^3 with the separation gaps of the width a of 0.3 mm was exposed to repetitive pulses of heat loads of $Q \sim 1.5$ MJ/m^2 and $\tau \sim 0.5$ ms with inclined plasma impact under the inclination

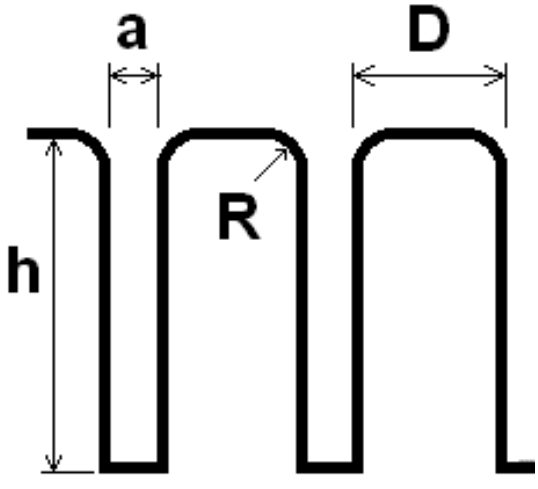

FIG. 3. Macro-brush target schematically

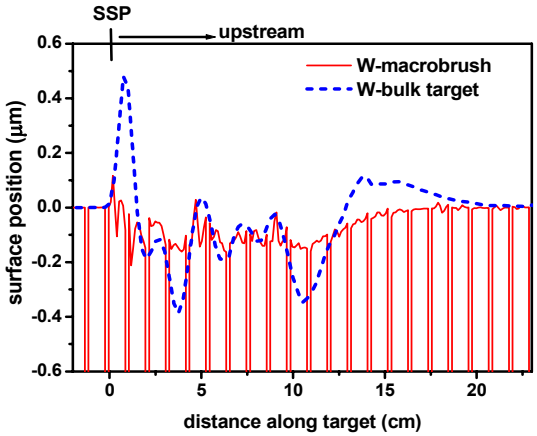

FIG. 4. Erosion of W-brush armour with a = 1 mm in comparison with that of bulk target (Q = 3.5 MJ/m^2, τ = 0.5 ms)

angle of 20 deg. The experimental profile was obtained to be well reproduced by the numerical simulations.

Several scenarios for single giant ELMs and single moderate disruptions are simulated. The W-macrobrush armour is assumed to consist of separate elements of sizes $D = 1$ cm, $R = 0.5$ mm, $a = 0.3$, 0.5 and 1 mm (see Fig. 3). In the test simulations the Lorentz force is omitted. Erosions of the macrobrush target and the bulk tungsten target are compared under the same heat load conditions. A giant ELM load with $Q = 3.5$ MJ/m^2 and $\tau = 0.5$ ms taken as the ITER reference scenario is modelled. The first disruption scenario corresponds to the mitigated disruption with $Q = 6$ MJ/m^2 and $\tau = 2$ ms. The second scenario corresponds to $Q = 15$ MJ/m^2 and $\tau = 5$ ms. The heat loads and plasma pressure distributions at the bulk tungsten target were calculated with FOREV-2D. In both scenarios the same peak energy flux at the target, of 3 GW/m^2, was obtained.

The MEMOS simulations of W-macrobrush armour damage under single ELM and the moderate disruptions demonstrated that radiation heat loads at the lateral surfaces of W−brushe are not sufficient for melting; the surface temperature at the top-brush- and arc segments coincides with that calculated for the bulk target. The W-brushes melt depth correlates well with that of the bulk target both for ELMs and disruptions. The maximum depth of the melt pool of 85 μm with length of 25 cm for giant ELMs achieves. In the first disruption scenario the maximum depth of the melt pool is obtained to be about 140 μm, with the pool length of 17 cm. For the second disruption scenario the depth increases up to 225 μm and the length up to 25 cm.

Plasma pressure gradient causes the melt motion with the melt velocity along the bulk target about 0.6 – 1 m/s whereas velocity of melt motion along the top-brush segments does not exceed 0.1 m/s for both ELMs and disruptions. Because of the rather small surface temperature at the lateral surface, the penetration of melted material into the gaps is negligible. The small sizes of W-brush faces prevent the violent melt motion and decrease the melt erosion of W-brush armour. In case of giant ELMs surface roughness of W-brush drops to 0.1 μm (see Fig. 4.) which is small compared to that 0.5 μm of the bulk target. For the giant ELMs the final erosion profile of the W-brush armour becomes comparable with the evaporation profile. In the case of moderate disruption the surface roughness increases up to 0.5 μm for the first scenario and up to 2.0 μm for the second one, which is due to much longer duration of the melt motion, remaining still much less than it is obtained for the bulk target (where the surface roughness of 1.2 μm and of 5 μm respectively was obtained). For the moderate disruptions the final erosion profile of the W-brush armour slightly exceeds the evaporation profile.

4. Enhanced erosion of CFC

The complicated structure of CFC is modelled in terms of involved properties: the thermal conductivity, the coefficient of thermal expansion and the Young's modulus. Three-dimensional structure of different sorts of graphite constitutes CFC. It includes a framework consisting of bunches of fibres and a matrix that fills the space between the tows. The pitch carbon fibres, perpendicular to the surface, provide high heat conductivity of CFC. They are woven and needled by the PAN fibres arranged parallel to the surface. CFC has good thermomechanical properties at surface temperatures at least up to 1.5×10^3 K [14], for instance a large thermal conductivity χ, in the fibres up to 10^3 W/mK. However, in average χ

is strongly anisotropic and varies from 10^2 to 3×10^2 W/mK. At the transient events the behaviour of CFC becomes problematic. For instance, CFC samples after irradiation by the plasma pulses of Q = 10 MJ/m^2 at $\tau \sim 0.05$ ms at MK–200UG and QSPA–T showed a drastic surface destruction with deep caverns of several hundred of μm and a strong damage along the longitudinal tows [15].

For analyses of the properties of CFC at the high heat fluxes the code PEGASUS–3D was applied [16]. The matrix and the tows are described by means of several millions of numerical cells of one-micrometer size. Some grains built of different groups of the cells simulate the graphite structure and the fibres. Neighbour cells contact by means of mechanical- and heat conduction bonds. In the simulations, the following typical parameters along and across the fibres are used: -1.5×10^{-6} and 20×10^{-6} K^{-1} for the thermal expansion coefficient, 500 and 20 GPa for the Young's modulus, 10^3 and 10^2 W/mK for the thermal conductivity, respectively.

Numerical simulations for NB31 using the Pegasus-3D code have explained the high erosion rate of NB31 by a new erosion mechanism due to local overheating [7]. The local overheating erosion mechanism (LOEM) has been found theoretically and needs experimental confirmation. Enhancement of erosion in LOEM is due to the preferential cracking on the interfaces between fibres and matrix followed by thermal isolation of the PAN fibres from the matrix and brittle destruction of the matrix there. In [16] investigation of CFC erosion under repetitive pulsed heat load simulating type I ELMs in ITER has been performed both numerically and experimentally.

Since the high heat loads are not achievable at the existing tokamaks, for estimation of divertor armour erosion the plasma guns MK-200UG [2] and QSPA [4] have been engaged.

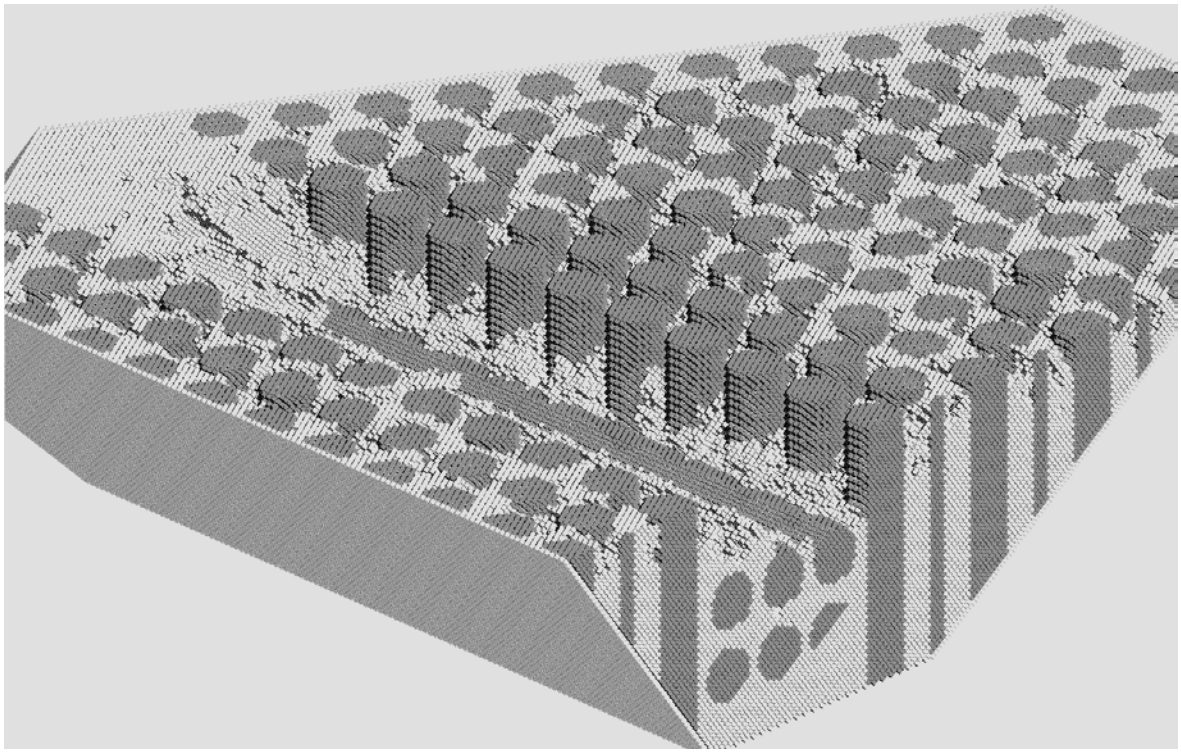

FIG.5. Erosion of CFC NB31 under ITER ELMs action. The valley is due to erosion of PAN fibres parallel to the sample surface and of the matrix surrounding them. Preferential erosion of the CFC at the site with PAN fibres and undermining of neighbouring pitch fibres (perpendicular to the surface) is seen. Erosion of the pitch fibres is negligible.

Corresponding numerical simulation has been done using the code Pegasus-3D. At MK-200UG the targets were irradiated by magnetized hydrogen plasma streams of the diameter d = 6 cm with energy density Q of 10-15 MJ/m^2 and the pulse duration $\tau = 40 - 50$ μs propagating along the magnetic field B of 2T. At QSPA, the samples were tested by the plasma streams with Q of 10 MJ/m^2, $d = 4$ cm, $\tau = 500$ μs and $B = 0$. At both facilities, the targets were exposed to perpendicular plasma impacts with the total number of plasma shots $N = 200$. Despite the fact that the plasma stream loads are of several times larger than it is expected for ITER ELMs the heat flux at the target surface is closer to the ELM conditions due to the vapour shield effect.

The experimental CFC erosion rate was obtained to be of a few microns per shot. Brittle destruction results in formation of open cavities at the CFC surface. The cavities are formed mainly along the PAN fibre bunches, which are parallel to the surface. With increase of number of plasma exposures, the cavities overlapped producing valleys along the PAN fibre bunches [15].

Because of considerable difference of the ELM simulation conditions in the plasma guns MK-200UG and QSPA from ITER impact the results of the experimentally determined erosion mechanism should be extrapolated on ITER ELM conditions. For this purpose numerical simulation using the code PEGASUS-3D has been performed. The results of the simulation are shown in Fig. 5. Most important fact is that under ITER ELM heating the CFC erosion is qualitatively the same as it has been observed in experiments on the plasma guns. Erosion of the PAN fibres, seen as a valley along the left side of the sample in the Fig.5 is much larger than the erosion in the pitch fibres region at the right side of the sample. Besides, erosion of the PAN fibres 'undermines' the matrix between the pitch fibres, stripping them at the boundary between the two regions.

5. Conclusions

In the radiation transport calculations for carbon impurity, the line radiation dominates. It is to note that the data for line shapes need further improvements, which demands significant effort for producing new opacities. Other facilities could be used for simulation. For instance, the experiments on the TEXTOR tokamak [17] have shown the radiative cooling of 20 keV per carbon atom and the tokamak several times ran into a disruption due to the artificial carbon influx into the core. Plasma diffusion in the pedestal and SOL should be taken into account in order to better estimate the density of carbon impurity in SOL and in the pedestal. For further validation of the code the measurements of the radiative cooling rate, of the amount of vaporised carbon and the electron temperature on JET tokamak during ELMs with the time resolution of ~10 μs are necessary.

The code MEMOS is further developed in the frame of "shallow water" approximation aiming to take into account the geometric peculiarities of W-brushes and melt motion at the gap edges. First validation of the code is performed against experiments on W-macrobrush target erosion under repetitive plasma loads. The experimental profile is well reproduced by the numerical simulations. The simulation demonstrated that for giant ELMs the W-macrobrush structure prevents violent melt motion: The velocity of melt motion drops more than for 3 times in comparison with the bulk armour and final erosion of the W-brush elements significantly decreases.

Further development of MEMOS is necessary, to take into account the real shape of brush elements for more accurate simulation of repetitive transient events. The validation of the code against surface temperature measurements at QSPA experiments could be useful.

Both experimental and numerical simulations resulted in the same erosion pattern for the NB31 CFC. The main features of theoretical LOEM have been confirmed experimentally. From the results of the simulations the conclusion follows that for a significant improvement of the CFC erosion strength against the ITER off normal events the structure of the CFC should have as less fibres parallel to the armour surface (e.g. weaving and needling fibres) as possible. The physical picture for CFC needs further development. PEGASUS-3D has to be validated against averaged thermophysical properties of CFC.

Acknowledgement

This work has been carried out within the research program of the European Task Force on Plasma-Wall interaction and partially funded by the task TW3-TPP-DISELM of the EFDA technology program.

References

[1] Federici et al., Journ. Nucl. Mat. 313-316 (2003) 11
[2] N.I. Arkhipov et al. J. Nucl. Mater. 233-237 (1996) 767
[3] V.I. Tereshin et al. J. Nucl. Mater. 313-316 (2003) 686
[4] V. Belan et al. Proc. 20th SOFT Marseille, France, 7-11 Sept. 1998, v.1, p. 101
[5] H. Wuerz et al. Fus. Sci. Techn. 40 (2001) 191
[6] B. Bazylev, H.Wuerz. Journ. Nucl. Mater. 307-311 (2002) 69
[7] S.E. Pestchanyi, H. Wuerz. Fus. Eng. Design, 66-68C (2003) 271
[8] S.E. Pestchanyi, I.S. Landman, H. Würz, "Hot plasma contamination in ELMs by divertor material", 30th EPS Conference on Contr. Fusion and Plasma Phys. St. Petersburg, 7-11 July 2003 ECA Vol. 27A, P-2.164 (compact disk)
[9] S. Pestchanyi, B. Bazylev and I. Landman. "Radiation losses from ITER SOL due to divertor material plasma", 31st EPS Conference on Plasma Phys. London, 28 June - 2 July 2004 ECA Vol.**28G**, P-1.135 (2004), avail. online: http://130.246.71.128/pdf/P1_135.pdf
[10] B. Bazylev, G.Janeschitz, I. Landman, S. Pestchanyi. "Erosion of divertor tungsten armor after many ELMs". Europhysics Conference Abstracts, Vol. **27A** (2003) P-2.44.
[11] B. Bazylev, G.Janeschitz, I. Landman, S. Pestchanyi. "Erosion of tungsten armor after multiple intense transient events in ITER", Proc. 16 Int. Conf. on Plasma Surface Interaction, Portland, USA, 2004, to appear.
[12] A. Zhitlukhin et al, "Effect of ELMs and disruptions on ITER divertor armour materials", Proc. 16 Int. Conf. on Plasma Surface Interaction, Portland, USA, 2004, to appear.
[13] B.N. Bazylev, G.Janeschitz, I.S. Landman, S.E. Pestchanyi. "Erosion of macrobrush tungsten armor after multiple intense transient events in ITER". Proc. 23rd Symposium on Fusion Technology, Venice, Italy, 2004, to be published
[14] J.P. Bonal, D. Moulinier. "Thermal properties of advanced carbon fiber composites for fusion application". Rapport DMT/95-495. CEA. Direction des reacteurs nucleaires. Departement de mecanique et de technologie (1995)
[15] I.S. Landman et al., Physica Scripta, T111 (2004) 206
[16] S.E. Pestchanyi et al., Journ. Nucl. Mater. 329-333 (2004) 697
[17] T. Scholz et al, J. Nucl. Mater. 241-243 (1997) 848